

Transmitter Point-Ahead using Dual Risley Prisms: Theory and Experiment

John Degnan (1), Jan McGarry (2), Thomas Zagwodzki (2), Thomas Varghese (3)

(1) Sigma Space Corporation

(2) NASA Goddard Space Flight Center

(3) Cybioms

John.Degnan@sigmaspace.com /Fax +01-301-577-9466

Abstract

For maximum detection efficiency and solar noise rejection, eyesafe photon-counting Satellite Laser Ranging (SLR) systems rely on narrow transmit beams and receiver FOV's. Because of the finite velocity of light, the transmit and receive FOV centers are angularly separated by up to 11 arcseconds in SLR and by several tens of arcseconds in interplanetary laser transponders or communications systems. We have successfully implemented and tested a dual Risley prism beam steerer for "Transmitter Point Ahead" (TPA) compensation in NASA's Next Generation Satellite Laser Ranging (NGSLR) System

Introduction

Conventional multiphoton SLR systems typically employ coaligned transmitters and receivers. The combination of high pulse energies, large transmitter beam divergences and even larger receiver fields-of-view ensure that a sufficient number of photons are reflected off the target and into the receiver to exceed the multiphotoelectron detection threshold. The latter is set sufficiently high (3 to 4 pe) to minimize false alarms under high solar background conditions. In contrast, eyesafe photon-counting systems operating at 532 nm in daylight must operate with over 3 orders of magnitude lower pulse energies, tight transmitter beam divergences to concentrate more of the transmitted light onto the satellite, and narrow receiver fields-of-view to reduce the solar background and improve the contrast between signal and solar noise.

As a consequence, the transmit and receive FOV's may no longer overlap if the point-ahead angle is sufficiently large. Thus, NASA's Next Generation Satellite Laser Ranging System (NGSLR, formerly known as SLR2000) is designed to point the receive telescope where the satellite was at the time the photons were reflected and independently point the transmitter ahead to where the satellite will be when the subsequent pulse arrives at the satellite (see Figure 1).

Overview of NGSLR Transceiver

The overall design and operation of the NGSLR transceiver has been described in prior workshops [Degnan, 2004], but a short overview is needed here to comprehend the nature of the "Transmitter Point-Ahead" (TPA) issue. Figure 2 provides a schematic of the NGSLR transceiver optical bench. The transmitter is input to a computer-controlled 5-element Special Optics beam expander which controls the final beam divergence while maintaining a constant beam spot size at the telescope exit aperture (for eye safety). This is followed by a Matched Dual Risley Prism Pair, which implements the TPA feature, and a passive T/R switch

consisting of an entrance polarizer, Faraday Isolator, half-wave plate and an exit polarizer. The reflected beam off the exit polarizer then passes through a 3-power beam expander and is reflected off the telescope pit mirror into a four mirror Coude system and an az-el tracking mount with a 40 cm aperture, x10.16 magnification, off-axis primary telescope.

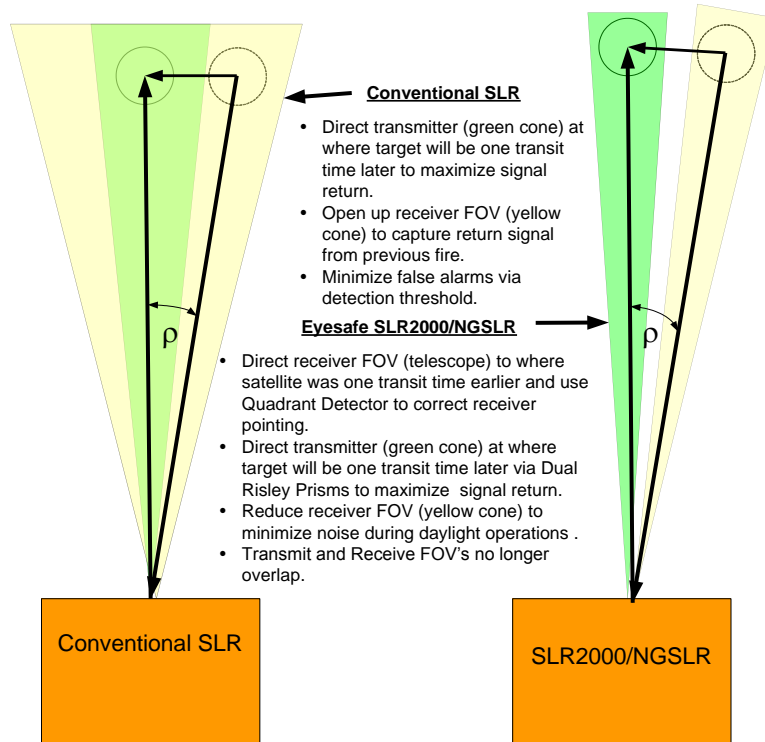


Figure 1. A comparison of conventional multiphoton SLR operations with that of the photon-counting SLR2000/NGSLR station.

Received photons are transmitted with high efficiency through the T/R switch (along two polarization paths) through the spectral and spatial filters to a quadrant MicroChannel Plate PhotoMultiplier Tube (MCP/PMT). Under full automated operation, signal count imbalances in the four quadrants are used to center the receive FOV on the “apparent” position of the satellite. The “apparent” position differs from the “true” position by the angular distance the satellite travels during the one-way transit of the reflected photons from the spacecraft to the station.

Coordinate Systems

The point-ahead angles expressed in the azimuth and elevation coordinates of the telescope, $\Delta\alpha$ and $\Delta\varepsilon$ respectively, are obtained from the orbit prediction program and are equal to the satellite angular rates in each axis multiplied by the roundtrip transit time of the light pulse. As shown in Figure 3a, we choose to express the TPA angle in polar coordinates as an angular magnitude, ρ , and direction, β_{AE} , as measured from the instantaneous telescope azimuth axis.

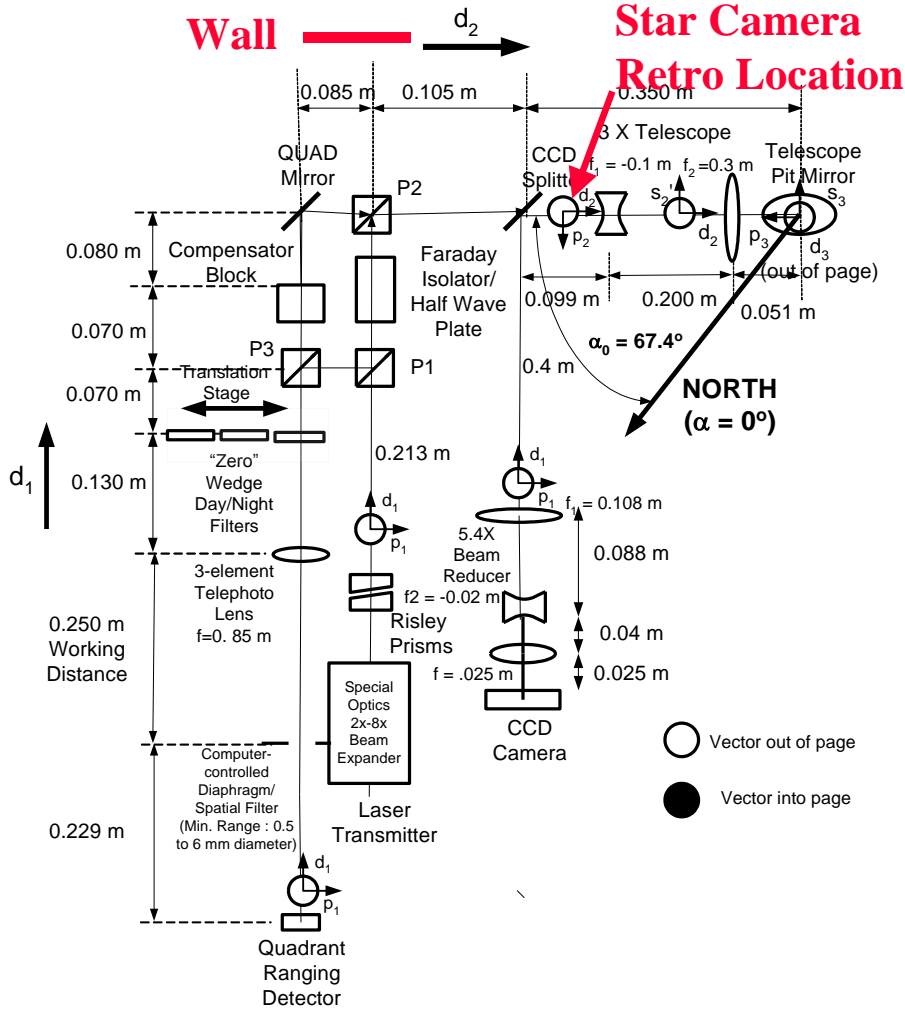


Figure 2. Block diagram of the NGSRLR transceiver optical bench. The positions of the “wall” and “star camera retro location”, referred to in the Experimental Validation Section , are superimposed in red.

Theoretical Predictions via Ray Tracing

Converting these az-el offsets into the proper rotation angle commands for the two Risley prisms requires that we properly account for the complex and time-dependent coordinate transformations that are imposed by the various optical components and the axis rotations of the Coude mount as the transmitted pulse travels from the Risleys to the exit aperture of the telescope. This was accomplished theoretically through “ray tracing” as described in a detailed internal report [Degnan, 2005]. We obtain for the rotation angle commands

$$\theta_5^c = \theta + \beta_{AE} + a \cos\left(\frac{\rho}{2R}\right) = \frac{\pi}{2} - \theta - \beta_{AE} + \frac{1}{2} a \cos\left[1 - \frac{(m_t \rho)^2}{2\delta^2}\right] \quad (1a)$$

$$\theta_6^c = \pi - \theta - \beta_{AE} + a \cos\left(\frac{\rho}{2R}\right) = -\frac{\pi}{2} + \theta + \beta_{AE} + \frac{1}{2} a \cos\left[1 - \frac{(m_t \rho)^2}{2\delta^2}\right] \quad (1b)$$

where the Coude θ -parameter

$$\theta = \alpha - \alpha_0 - \varepsilon + \frac{\pi}{2} = \alpha - \varepsilon + 22.5^\circ \quad (2)$$

takes into account the effect of the tracking mount on the orientation of the final TPA deflection. The parameters appearing in the above equations are: the instantaneous azimuth and elevation angles, α and ε ; a system specific azimuthal correction defined as the angle the input/output beam of the transceiver makes with the North direction as measured with a compass, $\alpha_0 = 67.5^\circ$ (see Figure 2); the overall effective magnification of the transmit beam following the Dual Risley Prisms, $m_t = 28.21$; and the deflection angle produced by a single wedge, $\delta \sim (n-1)w = 15.6$ arcmin, where n is the index of refraction and w is the wedge angle. The second form of the equations in (1) are currently used in the operational algorithms.

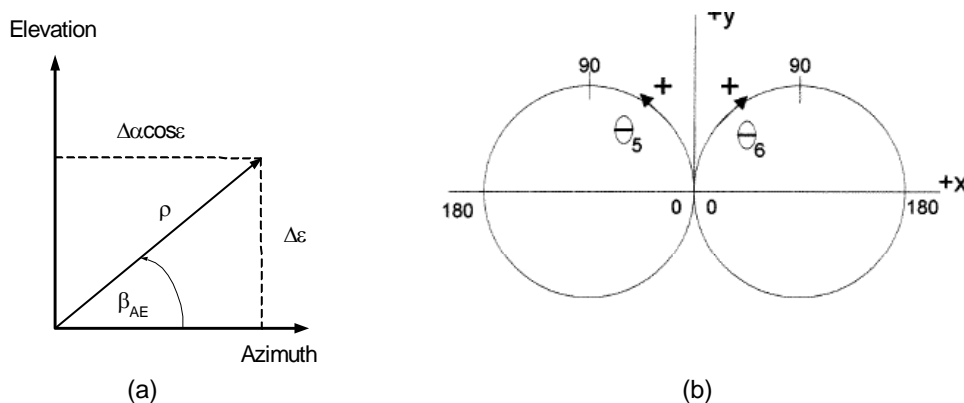


Figure 3. (a) TPA coordinate definitions in the instantaneous azimuth-elevation plane of the primary telescope. (b) Within the dual Risley unit, one wedge (θ_5) is rotated in a CCW direction from a “home” position along the positive x-axis while the second (θ_6) is rotated in a CW direction from a “home” position along the negative x-axis.

Experimental Validation

A simple, but low angular resolution, test was conducted by projecting the output of the dual Risley prism pair onto the “wall” directly behind the Risleys (see Figure 2) and at the telescope exit aperture for a fixed value of azimuth ($\alpha = 90^\circ$) and elevation ($\varepsilon = 22.5^\circ$) as a function of the commanded values of ρ and β_{AE} . In the experiments of Figure 4, ρ was constant at 10 arcsec, except for point J ($\rho = 0$), while β_{AE} took on the values 0, 90, 180, and 270° (F,G,H,I). As expected from (2), the telescope aperture pattern is rotated by $\theta = 90^\circ$ with respect to the wall pattern and the angular deviations are smaller by a factor $m_t = 28.21$.

Finally, for optimum performance, one must correct for any rotational angle biases between the “home” positions of the servo motor drivers and the corresponding wedge orientation. Retroreflecting the outgoing transmitter pulse from a point in the common transmit/receive path on the optical bench (labeled “Star Camera Retro Location” in Figure 2) into the focal plane of the star calibration camera, with a resolution of ~ 0.5 arcsec per pixel, allowed us to achieve the necessary angular sensitivity. The various parameters in the theoretical model were adjusted to give the “best” agreement with experiment as illustrated in Figure 5, where the abscissa and ordinate values correspond to the pixel numbers in the star camera.

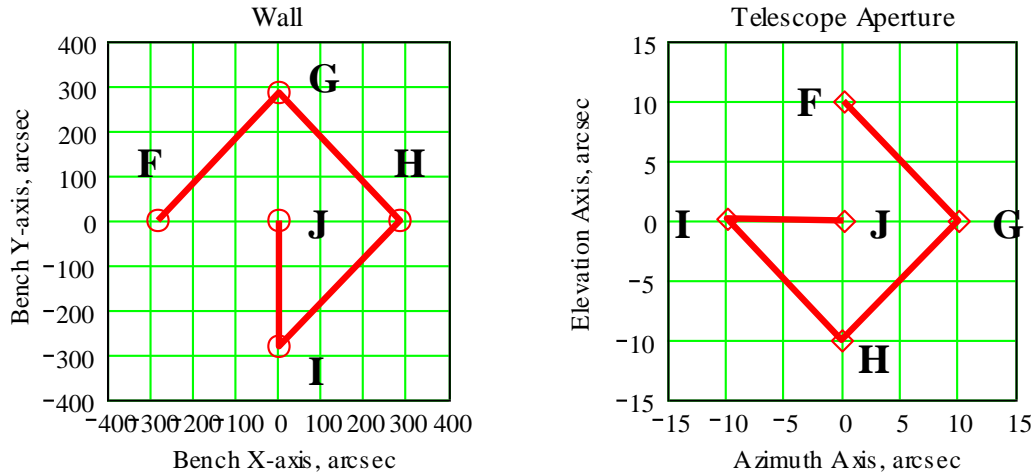


Figure 4. Projections of the deflected beam on the “wall” and at the telescope exit aperture. The pattern at the exit aperture is rotated by 90° in agreement with (2) for $\alpha = 90^\circ$ and $\varepsilon = 22.5^\circ$.

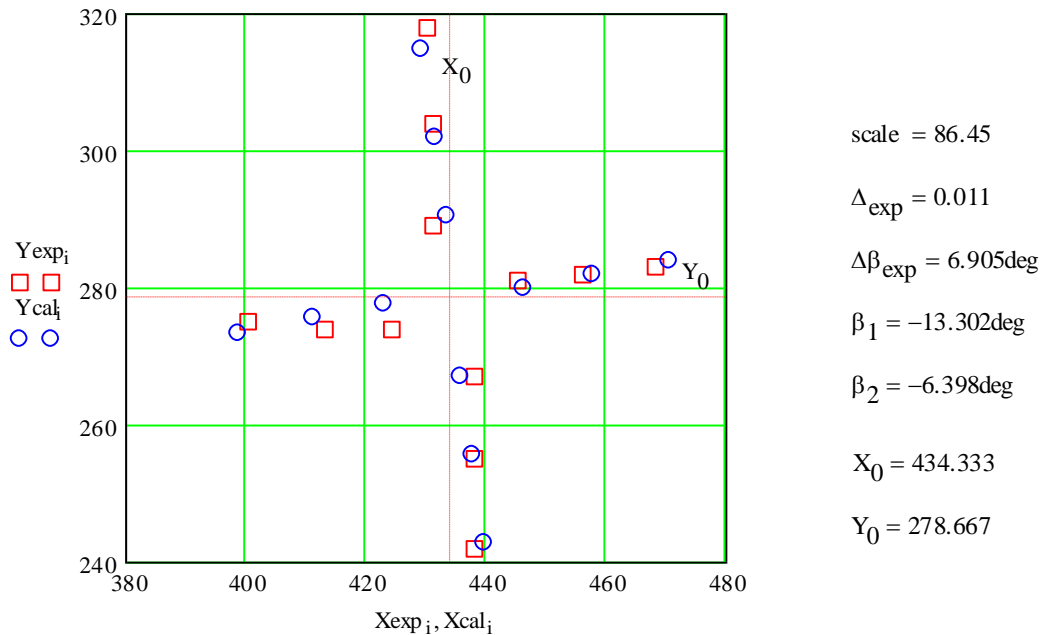


Figure 5. Star camera comparison of theory (blue diamonds) with experiment (red squares). Each major division (20 pixels) corresponds to slightly less than 10 arcsec.

The numerical values to the right of the plot correspond to the “best fit” values of the theoretical parameters to the experimental data. “Scale” is related to the mean deflection angle of each prism and sets the overall size of the pattern. Δ_{exp} is the fractional difference between the two wedge angles (1.1%), and the non-zero value is responsible for the open area near the origin defined by X_0 and Y_0 (intersecting vertical and horizontal red dashed lines) since, as mentioned previously, ρ cannot equal zero for unequal wedges. The parameters β_1 and β_2 are the rotational biases between the stepper motor “home” positions and the thick part of the wedge (i.e. direction of the individual wedge deflection), while $\Delta\beta_{\text{exp}}$ is simply the difference between the two rotational biases.

Summary

The development of the point-ahead algorithms for NGSLR was approached through an iterative combination of theoretical ray analyses and experiment until we achieved agreement. During the star camera experimentation, we found that the wedge angles of the two prisms differ by about 1.1%, implying that true “zero” deflection can never be achieved. However, ignoring this difference in the point-ahead algorithm produces an acceptable maximum transmitter pointing error of about 1.5 arcsec for small ρ . For larger ρ , the errors are typically sub-arcsecond. To avoid this small discrepancy in the future, tighter matching of the prism angles will be required.

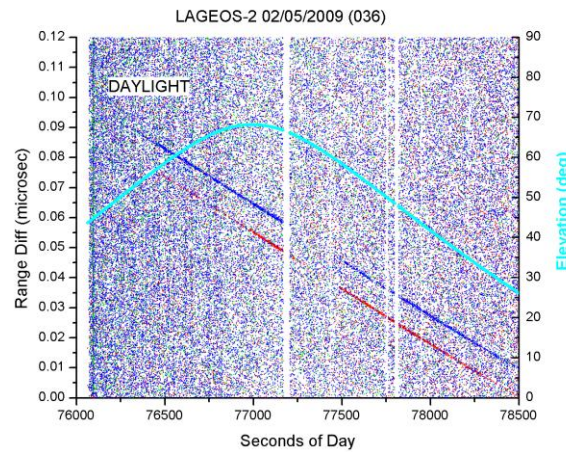


Figure 6. Daytime LAGEOS pass with time of day on the abscissa. The straight red and blue curves give the satellite returns in 2 of 4 quadrants offset by a fixed 100 nsec time delay. The magenta curve gives the satellite elevation on the right ordinate.

Since the workshop, we have successfully tracked LEO’s and LAGEOS in daylight with the Dual Risley TPA-mechanism active and the telescope pointing the receiver open loop to the apparent position of the satellite. Figure 6 shows a daylight LAGEOS pass which used a ± 2 arcsec transmit beam and a ± 5.5 arcsec receiver FOV. Maximum point-ahead for this pass was 7.8 arcsec. The blue and red lines in the plot correspond to the orbital fit from two different detector quadrants; the quadrants are offset from each other by 100 nsec so that all quadrant returns can be recorded by the Event Timer, which has a nominal 60 nsec deadtime. The absence of two quadrants in the plot is the result of not yet activating the closed loop pointing system (an upcoming NGSLR milestone) which attempts to derive receiver pointing corrections by balancing the count rates in the four detector quadrants.

Similar transmitter point-ahead systems and algorithms will be required for future interplanetary laser transponder and communications systems where the link margins are weak and ρ can take on values of several tens of arcseconds.

References

- Degnan, J. , 2004, “Ray Matrix Approach for the Real Time Control of SLR2000 Optical Elements”, Proc. 14th International Workshop on Laser Ranging, San Fernando, Spain, June 6-10.
- Degnan, J., 2005 ,“Ray Matrix Analysis for the Real-Time Control of Automated SLR2000 Subsystems”, Sigma Space Corporation Internal Report, October.